Electrical Quadruple Layer under the AC Electric Field

Yong Kweon Suh *

Department of Mechanical Engineering, Dong-A University,

840 Hadan-dong, Saha-gu, Busan 604-714, Korea

In this paper we show that solutions of the nonlinear Nernst-Planck equation possesses the quadruple-layer structure near the interface when the electrolyte receives a high frequency forcing such as a high-frequency alternating current. Very near to the interface wall, the well-known, classical Stern layer exists. Near to the Stern layer we have the secondly thin layer (to be called inner layer in this paper) where the ion concentrations behave under the same frequency as the external forcing. However, in this layer, the positive and negative ion concentrations develop with the time phase 180-degree different from each other. Next to this second layer, we have the third layer (called middle layer) in which two ion concentrations change with the time period double the forcing, and both concentrations behave in the same time phase. In the outermost layer, i.e. the forth layer, (called outer layer) the ion concentrations show the same-phase development as the third one but decaying very slowly in time. Our assertion is mostly based on the 1-D numerical simulation for the Nernst-Planck equation under a high frequency AC field assuming that the quadruple layer is very thin compared with the length scale representative of the bulk region.

Key Words: Electrical Double Layer, Electrical Quadruple Layer, Nernst-Planck Equation, Ion Transport

1. Introduction

It is well known that a solid surface when in contact with an electrolyte shows accumulation of ions (usually anions) at the interface due to some reason. Because of this, the counter ions (cations, in the usual cases) in the electrolyte are attracted to the region very close to the interface between the solid and liquid. Distribution of ions near the interface depends on the amount of ions adhered on the surface and also the nature of the electrolyte, such as PH and ion concentrations, etc. Figure 1 illustrates the concept sketch of this classical phenomenon.

*Corresponding Author,
E-mail :yksuh@dau.ac.kr
TEL : (51)200-7648; **FAX** : (51)200-7656
Department of Mechanical Engineering, Dong-A University,
840, Hadan-dong, Saha-gu, Busan 604-714, Korea

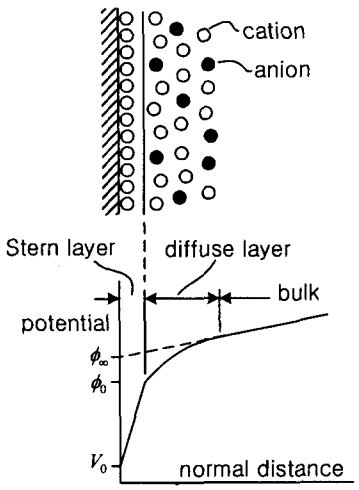

Fig. 1 Sketch of the EDL and potential change in each of three regions.

The thin layer called EDL(Electrical Double Layer) is known to be composed of basically two regions. The innermost layer is highly concentrated with the cations, and the ions are almost motionless because of the strong electrical force exerted from the solid wall. The remaining layer called diffuse layer has more cations than anions, and the ions can migrate from place to place. Therefore when an electric field is externally applied parallel to the interface, the mobile cations and anions in the diffuse layer move toward the positive and negative directions, respectively, of the external electric field. Since more cations are distributed in the layer than anions, the overall effect is fluid flow toward the positive direction of the electric field. The fluid velocity at the end of the diffuse layer is calculated by using the well known Helmholtz-Smoluchowski equation. Since in the microfluidc devices, the fluid is confined in a space with small length scales, the surrounding fluid particles is pulled immediately by the edge velocity, and for the channel case the velocity distribution takes a plug-type form. This effect is called electroosmosis.

There are numerous cases where we can explain the electrical or physical phenomena by using the EDL concept. Included in the phenomena are electroosmosis, electrophoresis, and di-electrophoresis, etc. These basic phenomena play key roles in the control of the microfluidic flows and particles manipulations, such as fluid pumping, fluid mixing, and particle assembly/trapping employed for a certain purpose such as biological detection.

The electroosmosis described above is an example of the EDL effect under a DC electric field. Very recently however increased attentions are given to the application of AC electric field in the microfluidic flow and particle controls. The response of EDL to the AC is more interesting and of course more dynamic than DC. We can use the forcing frequency as another control parameter, and so it is more feasible than using DC. Further, the electrode life becomes longer with AC. Use of metal electrodes together with AC in controlling particle assembly in small devices were reported not log ago. Trau et al. (1997) showed the long-range attraction of 2um-size particles on ITO electrodes, and they attributed such phenomenon to the hydrodynamic force given by the induced charge on the electrode. Green's group (Green and Morgan, 1998 and Ramos et al., 1998) reported separation of sub-micrometer particles on the array of electrodes, and they conjectured that heat generation and subsequent gradient of the conductivity and permittivity of the medium may induce the hydrodynamic force which results in the particle migration. One year later, they introduced the concept of AC electric-field-induced flow and electrode polarization to explain their experimental findings and proposed a simple capacitor model to verify the magnitude of the measured velocity. However the predicted velocity turned out to be much greater than the measured one. Another research group (Scott et al., 2001) attempted to fit the data of the Green's group and their theoretical model (Scott et al., 2000) without success. Later Green et al. (2002) refined their capacitor model by introducing another parameter representing the effect of potential drop across the compact (Stern) layer.

Lots of experimental evidence of the AC electroosmosis have been reported in association with the particle migration and assembly. Wong et al. (2004) fabricated a circular electrode surrounded by a circular strip of counter electrode and used PIV (particle image velocimetry) to measure the fluid velocity provided by the AC electroosmosis. The measured velocity shows dependence on the frequency and the electrolyte concentration. They also demonstrated the trapping of DNA molecules. Brown and Meinhart (2006) also conducted DNA-concentration experiment with a very similar electrode arrangement as Wong et al. (2004). Their numerical results are however two orders of magnitude greater than the measured ones and the predicted optimum frequency, at which the velocity becomes maximum, is also more than two orders of magnitude smaller than the experimental results. Several experiments on the evidence of particle aggregation along the center of electrode strips have also been reported (Zhou et al., 2005, Wu et al., 2005 and Lian et al., 2006). Bhatt et al. (2005) demonstrated the collection and concentration of latex particles and yeast cells around the patterned electrodes. Wong et al. (2004) review the various electrokinetic effects and their application in biotechnology. In most cases, the AC electroosmotic effect is naturally combined with the di-electrophoretic effect in control of the particles (e.g. Hoettges et al., 2003 and Gagnon and Chang, 2005).

The AC electroosmotic phenomena can be applied to various fields of microfluidics. By using anisotropic electrode arrays, Mpholo et al. (2003) showed that the plug-type flow profile can be achieved in pumping

fluid in a channel by placing two arrays of electrodes. Studer et al. (2002) presented the fabrication method for the pumping device using the AC electroosmosis. In order to pump fluids by using the AC electroosmotic effect, breaking of symmetry in the electric field (usually by using asymmetric geometry in the shape of electrodes themselves or in their arrays) are necessary. Bazant and Squires (2004) and Squires and Bazant (2005) give examples of electrode arrays for such purposes. The AC electroosmosis can also be used in fluid mixing. Wang et al. (2004) exhibited a turbulent-like mixing within a chamber containing a small conductive granule by applying DC and AC fields. They attribute the enhanced mixing to the vortices around the granule caused by the induced charge electroosmosis, as predicted by Bazant and Squires (2004). On the other hand, Wu et al. (2005) observed asymmetric flow patterns even with the symmetric electrode configuration, and they explained the phenomena in terms of the asymmetric-polarization, in which the Faraday reaction is to occur on the electrodes.

The basic ingredient of the above AC electroosmotic phenomena is the ion transport within the EDL. So, the very beginning point of the fundamental study on the AC electroosmosis should be the analysis on the ion transport in the layer. The governing equation for the ion transport within the EDL is the Nernst-Planck equation, which considers the ion diffusion and the ion migration in the dynamical system. As widely surveyed by Bazant et al. (2004), theoretical treatment of the Nernst-Planck equation goes back to Helmholtz. Since then the electrical effect of the EDL on the bulk electrolyte has been studied in terms of the development of electrical circuit model or simply the capacitor model representing the relation between the accumulation of charge in the EDL and the voltage drop across the EDL (refer to the literature given by Bazant et al., 2004 for the old references). The very recent theoretical touch on the Nernst-Planck equation was initiated by the group of Bazant in MIT. They considered the induced-charge electroosmosis around a conducting circular cylinder and showed that various flow patterns are possible depending on the externally applied electric field. They then applied their analytical method to the case of two oppositely facing planar electrodes (Bazant et al., 2004). Their important findings and possible applications are summarized in Bazant and Squires (2004). They also conducted a simple experiment for the case with a metal wire located within a microchannel receiving AC field. Their capacitor model however shows deviation from the experimental observation. On the contrary, the model of Green et al. (2002) fits the data well. They stress however that the physical ground of the model of Green et al. is questionable.

In this paper we propose the quadruple-layer structure instead of the double layer as the correct structure of the electrokinetic thin layer near the electrode surface. Our assertion is firstly based on the numerical solution to the 1-D Nernst-Planck equation, and then it is verified from the asymptotic solutions for each layer.

2. Governing Equations

Governing equations for the concentrations are

$$\frac{\partial c^{*\pm}}{\partial t^*} + \mathbf{u}^* \cdot \nabla^* c^{*\pm} = D\left[\nabla^{*2} c^{*\pm} \pm \left(\frac{ze}{k_b T}\right)\nabla^* \cdot \left(c^{*\pm}\nabla^*\phi^*\right)\right] \quad (1)$$

$$\varepsilon\varepsilon_0 \nabla^{*2}\phi^* = -\rho_e^* \quad (2)$$

$$\rho_e^* = (c^{*+} - c^{*-})ze \quad (3)$$

where t^* is the time [s], c^{*+} and c^{*-} the local concentration of positive and negative ions, i.e. number of ion molecules per volume of the electrolyte solution [1/m^3], $\mathbf{u}^*$ the fluid velocity vector [m/s], ϕ^* the local electric potential [V], ρ_e^* the electric charge density [C/m^3], and x^*, y^* the spatial coordinates [m]. Further, D is the ion diffusivity [m^2/s], z the valence of the (symmetric) ions, e the electron charge(1.60×10^{-19}) [C], k_b the Boltzmann constant (1.38×10^{-23}) [J/K], T the temperature [K], ε the dielectric constant, and ε_0 the permittivity of vacuum (8.85×10^{-12}) [C^2/Nm^2]. The variables are scaled as follows; $(x^*, y^*) = L(x, y)$, $t^* = t/\omega$, $\mathbf{u}^* = U_s\mathbf{u}$, $c^{*\pm} = c_0^* c^{\pm}$, $\phi^* = \phi_{ref}^*\phi$, and $\rho_e^* = c_0^* z e \rho_e$. Here, the reference quantities are; L the reference length such as distance between the electrodes [m], ω the angular frequency of the AC potential [1/s], U_s the Helmholtz-Smoluchowski velocity based on the thermal potential and the external electric field ($\varepsilon\varepsilon_0\varsigma^* V_{00}^*/\mu L$) [m/s], ς^* the thermal potential ($k_b T/ze$) [V], V_{00}^* the amplitude of the external AC potential applied on the pair of electrodes [V], μ the dynamic viscosity of the fluid [Ns/m^2], c_0^* the bulk concentration of ions (number density) [1/m^3], ϕ_{ref}^* the reference potential ($(L/\lambda_d)^2(D/L^2\omega)\varsigma^*/2$), and $\lambda_d = \sqrt{\varepsilon\varepsilon_0 k_b T/2c_0^* z^2 e^2}$ the Debye screening length or EDL thickness [m]. Then the equations take the form

$$\frac{\partial c^{\pm}}{\partial t}+\varepsilon_1 \mathbf{u}\cdot\nabla c^{\pm}=\varepsilon_3^2\left[\nabla^2 c^{\pm}\pm\gamma\nabla\cdot\left(c^{\pm}\nabla\phi\right)\right] \quad (4)$$

$$\varepsilon_3^2\nabla^2\phi=-\rho_e \quad (5)$$

$$\rho_e=(c^+-c^-) \quad (6)$$

where dimensionless parameters are

$\gamma=\phi^*_{ref}/\varsigma^*=(L/\lambda_d)^2\varepsilon_3^2/2$,

$\varepsilon_1=U_s/\omega L$, $\varepsilon_3=\sqrt{D/L^2\omega}$.

We are interested in the case of small ε_1, such that the convective terms can be neglected. We expect a thin layer (i.e. 'screening layer' and called EDL), which we will call EQL in this paper, and the bulk region. Ions are expected to be neutralized in the bulk region, and so the Laplace equation governs the potential distribution.

$$\nabla^2\phi=0 \quad (7)$$

For a typical example, we assume the potential difference between the pair of electrodes, $V^*_{00}=1$ [V] and the reference length, $L=20$ [um]. Further we assume $\omega=100$ [rad/s], $D=10^{-10}$ [m^2/s] and $T=300$ [K]. For the bulk concentration, we assume 10^{-3} [M] of KCl solution. Then we get $\varsigma^*=26$ [mV] and $\gamma=5260$. Notice that the value of γ is very large for this typical case.

To resolve the EQL, we introduce the strained coordinate along the direction normal to the electrode surface; $n=\sqrt{2\varepsilon_3}Y$. Then the concentration equations and the potential equation become

$$2\frac{\partial c^{\pm}}{\partial t}=\frac{\partial^2 c^{\pm}}{\partial Y^2}\pm\gamma\frac{\partial}{\partial Y}\left(c^{\pm}\frac{\partial\phi}{\partial Y}\right) \quad (8)$$

$$\frac{\partial^2\phi}{\partial Y^2}=-c^++c^- \quad (9)$$

We need boundary conditions. On the electrode surface the current flux should vanish.

$$J^+=\frac{\partial c^+}{\partial Y}+\gamma c^+\frac{\partial\phi}{\partial Y}=0 \quad \text{at } Y=0 \quad (10a)$$

$$J^-=\frac{\partial c^-}{\partial Y}-\gamma c^-\frac{\partial\phi}{\partial Y}=0 \quad \text{at } Y=0 \quad (10b)$$

As for the boundary condition for the potential, we employ the Stern-layer capacitor model. Let C^*_S the Stern-layer capacitance and λ_S the Stern-layer thickness. Then the amount of charge in the screening layer q^* is given by

$$q^*=C^*_S(\phi^*-V^*_{00}\cos t) \quad (11)$$

On the other hand, the capacitance C^*_S is computed from

$$C^*_S=\frac{\varepsilon_S\varepsilon_0}{\lambda_S} \quad (12)$$

where ε_S is the dielectric constant of the Stern layer. The charge is given by integration of the charge density over the diffuse layer

$$q^*=\int_0^\infty\rho_e^*dn^*=-\varepsilon\varepsilon_0\int_0^\infty\frac{\partial^2\phi^*}{\partial n^{*2}}dn^*=\varepsilon\varepsilon_0\left[\left(\frac{\partial\phi^*}{\partial n^*}\right)_0-\left(\frac{\partial\phi^*}{\partial n^*}\right)_\infty\right] \quad (13)$$

where $n^*=0$ indicates the interface between the Stern layer and the diffuse layer, and $n^*=\infty$ the outer edge of the diffuse layer. Substituting (12) and (13) into (11) we get

$$\phi_0=\varepsilon_5\left[\left(\frac{\partial\phi}{\partial Y}\right)_0-\left(\frac{\partial\phi}{\partial Y}\right)_\infty\right]+V_{00}\cos t \quad (14)$$

where V_{00} is the scaled quantity of V^*_{00}, i.e. $V_{00}=V^*_{00}/\phi^*_{ref}$, and $\varepsilon_5=\lambda_S\varepsilon/\varepsilon_S/\sqrt{2\varepsilon_3}L$. The numerator in the equation for ε_5 corresponds to the equivalent thickness of the Stern layer. Note that the gradient of the potential at the outer edge of the EQL also participates in the boundary condition for the potential at the inner edge of the layer.

As the boundary conditions at the outer edge of the layer, we simply assume that the bulk concentrations are not disturbed; $c^+=c^-=1$ at $Y=\infty$. As for condition of the potential, we assume non-zero but a constant gradient; $\partial\phi/\partial Y=$ function of time at $Y=\infty$. Note that with zero gradient for this yields zero current flux at the outer edge, and so no dynamic behavior of the charge or potential is expected to occur within the layer.

3. Asymptotic solutions of the EQL equations for very large γ

When the parameter γ is of order 1 or larger, the linear solutions may not hold and we must ultimately rely on the numerical solutions for the full EQL equations. However in order to determine the slip velocity at the outer edge of the EQL effectively, we must develop a very simple formula which can be combined with the solution in the bulk region through a suitable interaction algorithm. In this section we present the asymptotic solutions applicable when γ is very large.

From the beginning we must rely on the numerical results that at very large γ values, the solutions show three kinds of distinctly different behavior at each of three layers as shown in Fig. 2. To obtain these numerical results we applied the following parameter

Fig. 3(a). In this layer the potential gradient Φ becomes 100 times the forcing one supplied from the bulk region; compare the magnitude of Φ at Fig. 2(b) and that at Fig. 2(d) or Fig. 3(f). However, the evolution of Φ shows the 90-degree different phase from the forcing one. It should be also mentioned that although the difference between c^+ and c^- is considerable, the magnitude of Φ is not so large. This can be understood from the following equation.

$$\frac{\partial \Phi}{\partial Y} = -c^+ + c^-, \qquad (15)$$

which can be derived from Eq. (9) and definition of Φ, showing that Φ is the integration result of the difference between c^+ and c^-. Since the inner layer thickness is very small, the integrated result cannot be large even though the integrand is considerable.

In the middle layer, the evolution of each of the three variables is as shown in Fig. 2(c), (d) and Fig. 3(b); here the development of c^- is the same as that of c^+ shown in Fig. 2(c) with the same phase. Both the concentrations also show the asymptotic approach toward 1 but the potential gradient shows almost constant values (in fact at the same magnitude as the forcing one). Peculiar in this layer is that the two concentrations show almost the same behavior and that the time period is half the forcing one as can be seen from Fig. 3(b). Perturbed concentrations are much smaller than those of the inner layer but much larger then the outer layer; compare $(c^{\pm} - 1)$ in Fig. 3(b) and the one in Fig. 3(c). In this layer the potential gradient shows the same time-phase as the forcing one. In the outer layer, the concentrations do not show the harmonic motions in time, and they asymptotically approach to 1 at infinity; see Fig. 2(e). As can be seen from Fig. 3(c) the variation of these concentrations is very small during one period of time. The behavior of the potential gradient in this layer is the same as that at the middle layer; compare Fig. 2(f) and Fig. 2(d). Figure 4 shows the time evolution of c^+ in the outer layer for 50 periods. The profile of c^- is not plotted in this figure because it is almost the same as that of c^+ in this layer. It reveals that the evolution is purely diffusive.

To catch the order of the magnitude in each region we computed each term of the Nernst-Planck equation separately and compared with each other. The results indicate that within the inner layer the transient term is very small and the governing equations show balance between the ion diffusion and ion migration terms. This implies that the inner layer has the characteristic time very short compared with the time scale selected in this study, i.e. $1/\omega$. In the middle and outer layers the ion migration term can be neglected. The trend of above comparison is more pronounced as γ is increased.

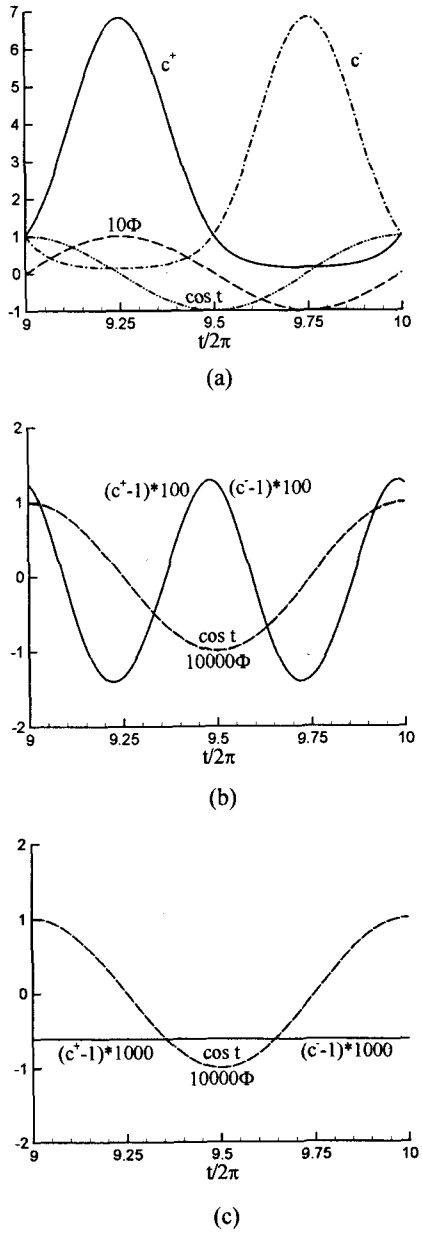

Fig. 3 Time series of the concentrations c^+, c^- and the potential gradient Φ at three locations; (a) $Y = 0$, (b) $Y = 0.374$ and (c) $Y = 9.01$.

Based on our numerical results, we propose the following form of approximated equations, instead of the full equations (8), as the appropriate equations governing the ion transport in each of the three layers.

$$\frac{\partial^2 c^{\pm}}{\partial Y^2} \pm \gamma \frac{\partial}{\partial Y}\left(c^{\pm} \frac{\partial \phi}{\partial Y} \right) = 0 \quad \text{for the inner layer} \qquad (16a)$$

$$2\frac{\partial c^{\pm}}{\partial t} = \frac{\partial^2 c^{\pm}}{\partial Y^2} \quad \text{for the middle and outer layers.} \qquad (16b)$$

These equations are to be solved together with (9).

To obtain the analytic solutions of the inner layer equations, we first multiply (9) by Φ and integrate once to get

$$c^+ + c^- = \frac{\gamma}{2}(\Phi^2 - \Phi_\infty^2) + 2 \qquad (17)$$

where Φ_∞ corresponds to the asymptotic value of Φ at infinity. At moment we neglect this term. Then from (16a), we derive

$$\frac{\partial (c^+ - c^-)}{\partial Y} + \gamma (c^+ + c^-)\Phi = 0$$

Next we apply (9) and (17) to this equation to obtain the equation for Φ only as follows.

$$\Phi'' = \gamma \Phi \left(\frac{\gamma}{2}\Phi^2 + 2 \right)$$

where prime denotes $\partial / \partial Y$. This can be integrated once to give

$$\Phi' = -\sqrt{2\gamma}\,\Phi \sqrt{\frac{\gamma}{8}\Phi^4 + \Phi^2 - \frac{\gamma}{8}\Phi_\infty^4 - \Phi_\infty^2} \qquad (18)$$

where the negative sign was selected considering the asymptotic nature at infinity. Here again we neglect the terms with Φ_∞. This then can be integrated once more to yield

$$\Phi = \frac{\sqrt{8/\gamma}}{\sinh[\sqrt{2\gamma}(Y + Y_0)]} \qquad (19)$$

where the integration constant $Y_0(t)$ should be determined from a certain restriction. The solutions for $c^{\pm}$ can be obtained by substituting (19) into (16a). The results are

$$c^{\pm} = \frac{\cosh[\sqrt{2\gamma}(Y + Y_0)] \pm 1}{\cosh[\sqrt{2\gamma}(Y + Y_0)] \mp 1} \qquad (20)$$

Now to determine the function $Y_0(t)$, we may use the integral relation

$$2\int_0^\infty \frac{\partial c^+}{\partial t} dY = J_\infty^+ \qquad (21)$$

which can be derived from the full equation (8), but it turned out the ion distributions in the middle and outer layers play important roles in the evaluation of the left-hand side term. In order to determine $Y_0(t)$ more practically, we rely again on the numerical results of the full governing equations. We notice that the behavior of Φ is very closely harmonic in time as shown in Fig. 3(a). So we assume that $\Phi = \Phi_0 \sin t$ at $Y = 0$. Then from (19) we readily obtain

$$Y_0 = \frac{1}{\sqrt{2\gamma}} \sinh^{-1}\left(\frac{\sqrt{8/\gamma}}{\Phi_0 \sin t} \right) \qquad (22)$$

Substituting this into (20) results in the explicit expression for the concentrations;

$$c^{\pm} = \frac{\sqrt{8/\gamma + \Phi_0^2 \sin^2 t}\,\cosh(\sqrt{2\gamma}Y) + \sqrt{8/\gamma}\sinh(\sqrt{2\gamma}Y) \pm \Phi_0 \sin t}{\sqrt{8/\gamma + \Phi_0^2 \sin^2 t}\,\cosh(\sqrt{2\gamma}Y) + \sqrt{8/\gamma}\sinh(\sqrt{2\gamma}Y) \mp \Phi_0 \sin t} \qquad (23)$$

We also have an explicit expression for Φ_0;

$$\Phi = \frac{\sqrt{8/\gamma}\,\Phi_0 \sin t}{\sqrt{8/\gamma + \Phi_0^2 \sin^2 t}\,\sinh(\sqrt{2\gamma}Y) + \sqrt{8/\gamma}\cosh(\sqrt{2\gamma}Y)} \qquad (24)$$

Now the question is; how to determine the constant Φ_0? For this we first apply the inner-layer solution (20) to the constraint (21) to obtain

$$2\int_0^\infty \frac{\partial c^+}{\partial t} dY = \gamma A_\infty' \cos t \qquad (25)$$

Substituting (20) into the left-hand side gives

$$\text{LHS} = \Phi_0 \cos t \left(1 + \frac{\Phi_0 \sin t}{\sqrt{8/\gamma + \Phi_0^2 \sin^2 t}} \right) \qquad (26)$$

which can be written in the Fourier expansion form as

$$\text{LHS} = \sum_{n=1}^{\infty} (a_n \cos nt + b_n \sin nt) \qquad (27)$$

We can show that $a_1 = \Phi_0$, $a_n = 0$ ($n = 2,...$) , and $b_1 = b_3 = b_5 = ... = 0$. This indicates that the requirement (25) can be satisfied only with the fundamental mode, and the higher modes must be treated elsewhere; in fact the remaining terms are treated by the middle layer solutions. Then we obtain $\Phi_0 = \gamma A_\infty'$.

Similarly the constraint for c^- is

$$2\int_0^\infty \frac{\partial c^-}{\partial t} dY = -\gamma A_\infty' \cos t \qquad (28)$$

and we end up with the following relation.

$$\Phi_0 \cos t \left(-1 + \frac{\Phi_0 \sin t}{\sqrt{8/\gamma + \Phi_0^2 \sin^2 t}} \right) = -\gamma A_\infty' \cos t \qquad (29)$$

The fundamental mode results in (27) and the remaining modes are the same as before. This means that in the middle layer, the function c^+ should be the same as c^-.

In the middle layer, the equation to be solved is (16b)

which is linear. For a positive real constant λ, we can write the general solution as

$$c^{\pm} = C\exp[-\lambda Y + i(\lambda^2 t - \lambda Y)]$$

where C is an arbitrary complex constant, and taking the real part is assumed. The constants C and λ are determined from the following requirement.

$$2\int_0^{\infty} \frac{\partial c^{\pm}}{\partial t} dY = -b_2 \sin 2t + \ldots \quad (30)$$

where the higher modes are composed of terms like $\sin 4t$ etc. and in most cases these terms can be neglected. Then we get the following as the solution of $c^{\pm}$ for the middle layer.

$$c^{\pm} = c_c^{\pm} + \frac{b_2}{2}\exp(-\sqrt{2}Y)\cos(2t - \sqrt{2}Y + \pi/4) \quad (31)$$

Note that the constant $c_c^{\pm}$ is added to consider the effect of the outer-layer solution.

In the outer layer, the equation to be solved is again (16b). Existence of the outer layer comes from the following requirement

$$\text{time average of}\left[2\int_0^{\infty}(c^{\pm}-1)dY\right] = \text{constant} \quad (32)$$

If the initial distribution of $c^{\pm}$ is just $c^{\pm}=1$ as is the usual case, then the constant must be zero. In fact the inner-layer solution of $c^{\pm}$ shows that $c^{\pm}-1$ has significant amount of steady components as shown from Fig. 2(a). Substituting (20) into the left-hand side of (32) gives

$$\alpha_0 = \frac{1}{2}\left(\frac{1}{2\pi}\int_0^{2\pi}\sqrt{8/\gamma + {\Phi_0}^2 \sin^2 t}\, dt - \sqrt{8/\gamma}\right) \quad (33)$$

Now the outer-layer solution must take care of this non-zero value of α_0. The general solution to (16b) having this purpose can be written as follows.

$$c^{\pm} = 1 + \frac{C_1 \exp(-\eta^2)}{\sqrt{2t}}$$

where $\eta = Y/\sqrt{2t}$. The constant C_1 is determined from the requirement

$$2\int_0^{\infty}(c^{\pm}-1)dY = -\alpha_0$$

and get $C_1 = -2\alpha_0/\sqrt{\pi}$. Then the final form of the outer-layer solution is

$$c^{\pm} = 1 - \frac{2\alpha_0 \exp(-\eta^2)}{\sqrt{2\pi t}} \quad (34)$$

The analytical solutions in the inner, middle and outer layer are compared with the numerical solutions in Fig. 2(a), 2(c) and Fig. 4, respectively. It is remarkable to note that comparison is much more satisfactory than expected. Being satisfied with the accurate prediction of the solutions provided by the analytical formula, our next step is to construct an algorithm which can predict through a suitable interaction scheme the true potential drop across the EQL and simultaneously the potential gradient at the outer edge of the EQL.

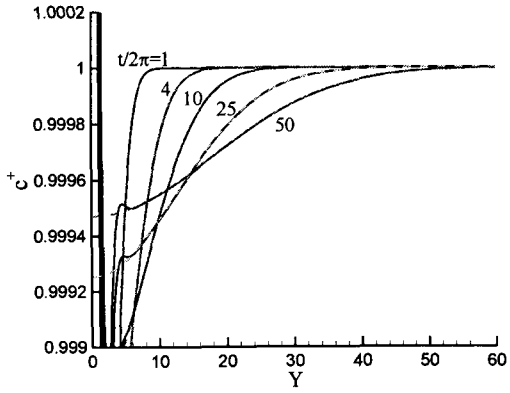

Fig. 4 Comparison between the numerical (solid lines) and asymptotical solutions of c^{+} within the outer layer.

5. Conclusions

We have shown, with the aid of numerical simulation, that the Nerns-Planck equations intrinsically contain quadruple-layer solutions at large values of the parameter γ, when the layer is receiving AC potential. We have encountered no problem in matching solutions between each pair of the neighboring layers. The inner layer is the thinnest among the three layers (excluding the Stern layer), and in this layer the concentrations develop in time with a strongly non-harmonic behavior. The positive and negative ion concentrations show the temporal behavior with the time phase 180-degree different from each other. The potential gradient shows however an almost harmonic behavior in this layer. In the middle layer both the positive and negative ion concentrations develop in the same magnitude and same time phase, so the potential gradient does not show spatial change in the middle layer. This layer however shows the temporal oscillation of the concentrations with the period double the forcing one. This layer can be considered as a reservoir supplying to or receiving from the inner layer the higher harmonic components of the ion charges. The outer layer is characterized by a slow diffusion of the excess

concentrations which were initiated by the initial conditions or the non-zero steady components developed from the beginning in the inner layer. In this layer too, the potential gradient does not show any spatial change, because the positive and negative ion concentrations are the same.

Acknowledgement

This work was supported by National Research Laboratory Program provided by KOSEF.

References

Bazant, M.Z. and Squires, T.M., 2004, "Induced-charge electrokinetic phenomena: Theory and microfluidic applications", *Phys. Rev. Lett.*, Vol. 92, No. 6, 066101.

Bazant, M.Z., Thornton K. and Ajdari, A., 2004, "Diffuse-charge dynamics in electrochemical systems", *Phy. Rev E*, Vol. 70, 021506.

Bhatt, K.H., Grego, S. and velev, O.D., "An AC electrokinetic technique for collection and concentration of particles and cells on patterned electrodes", *Langmuir*, Vol. 21, pp. 6603-6612.

Brown, M.R. and Meinhart, C.D., 2006, "AC electroosmotic flow in a DNA concentrator", *Microfluid Nanofluid*, DOI 10.1007/s10404-006-0097-4.

Gagnon, Z. and Chang, H.-C., 2005, "Aligning fast alternating current elexctroosmotic flow fields and characteristic frequencies with dielectrophoretic traps to achieve rapid bacteria detection", *Electrophoresis*, Vol. 26, pp. 3725-3737.

Green, N.G. and Morgan, H., 1998, "Separation of submicrometer particles using a combination of dielectrophoretic and electrohydrodynamic forces", *J. Phys. D: Appl. Phys.* Vol. 31, L25-L30.

Green, N.G., Ramos, A., Gonzalez, A., Morgan, H. and Castellanos, A., 2002, "Fluid flow induced by nonuniform ac electric fields in electrolytes on microelectrodes. III. Observation of streamlines and numerical simulation", *Phys. Rev. E*, Vol. 66, pp. L25-L30.

Hoettges, K.F., McDonnell, M.B. and Hughes, M.P., "Use of combined dielectrophoretic/electro-hydrodynamic forces for biosensor enhancement", *J. Phys. D: Appl. Phys.*, Vol. 36, p. L101-L104.

Lian, M., Islam, N. and Wu, J., "particle line assembly/patterning by microfluidic AC electroosmosis", *J. Phys: Conf. Series* Vol. 34, pp. 589-594.

Mpholo, M., Smith, C.G. and Brown, A.B.D., 2003, "Low voltage plug flow pumping using anisotropic electrode arrays", *Sensors and Actuators* B, Vol. 92, pp. 262-268.

Ramos, A., Morgan, H., Green, N.G. and Castellanos, A., 1998, "Ac electrokinetics: a review of forces in microelectrode structures", *J. Phys. D: Appl. Phys.* Vol. 31, pp. 2338-2353.

Scott, M., Kaler, K.V.I. and Paul, R., 2001, "Theoretical model of electrode polarization and AC electroosmotic fluid flow in planar electrode arrays", *J. Colloid and Interface Sci.*, Vol. 238, pp. 449-451.

Scott, M., Paul, R. and Kaler, K.V.I., 2000, "Theory of frequency-dependent polarization of general planar electrodes with zeta potentials of arbitrary magnitude in ionic media", *J. Colloid and Interface Sci.*, Vol. 230, pp. 377-387.

Squires, T.M. and Bazant, M.Z., 2005, "Breaking symmetries in induced-charge electro-osmosis and electrophoresis", *J. Fluid Mech.*, Vol. 560, pp. 65-101.

Studer, V., Pepin, A., Chen, Y. and Ajdari, A., 2002, "Fabrication of microfluidic devices for AC electrokinetic fluid pumping", *Microelectronic Eng.*, Vol. 61-62, pp. 915-920.

Trau, M., Savile and Aksay, I.A., 1997, "Assembly of colloidal crystals at electrode interfaces", *Langmuir*, Vol. 13, pp. 6375-6381.

Wang, S.-C., Lai, Y.-W., Ben, Y. and Chang, H.-C., 2004, "Microfluidic mixing by dc and ac nonlinear electrokinetic vortex flows", *Ind. Eng. Chem. Res.*, Vol. 43, pp. 2902-2911.

Wong, P.K., Chen, C.-Y., Wang, T.-H. and Ho, C.-M., 2004, "Electrokinetic bioprocessor for concentrating cells and molecules", *Anal. Chem.*, Vol. 76, p. 6908-6914.

Wong, P.K., Wang, T.-H., Deval, J.H. and Ho, C.-M., 2004, "Electrokinetics in micro devices for biotechnology aplications", *AIEEE/ASME Trans. Mechatronics*, Vol. 9, No. 2, pp. 366-376.

Wu, J., Ben, Y., Battigelli, D. and Chang, H.-C., "Long-range AC electroosmotic trapping and detection of bioparticles", *Ind. Eng. Chem. Res.*, Vol. 44, pp. 2815-2822.

Wu, J., Ben, Y. and Chang, H.-C., "Particle detection by electrical impedance spectroscopy with asymmetric-polarization AC electroosmotic trapping", *Microfluid Nanofluid*, Vol. 1, pp. 161-167.

Zhou, H., White, L.R. and Tilton, R.D., "lateral separation of colloids or cells by dielectrophoresis augmented by AC electroosmosis", *J. Colloid and Interface Sci.*, Vol. 285, pp. 179-191.

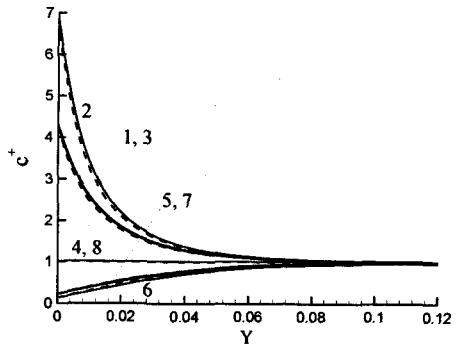

(a)

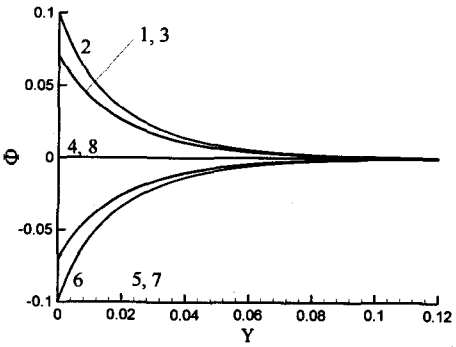

(b)

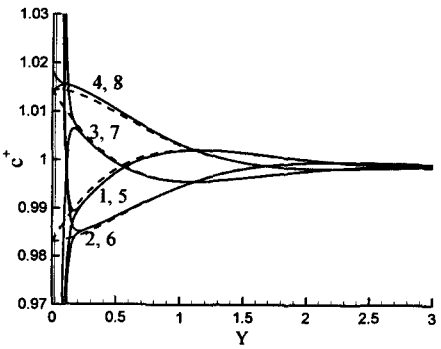

(c)

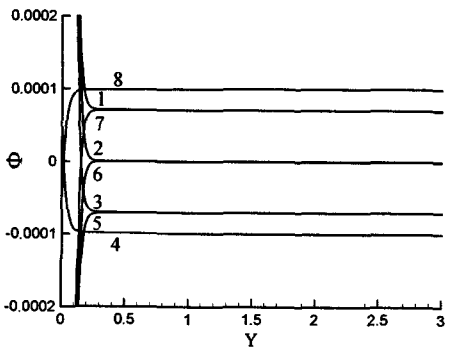

(d)

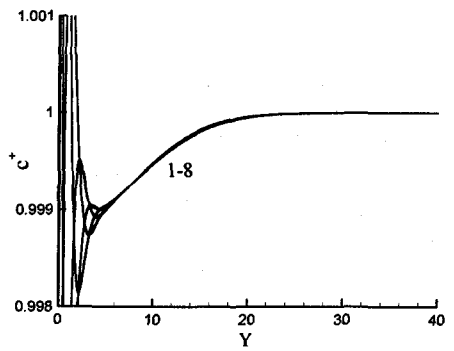

(e)

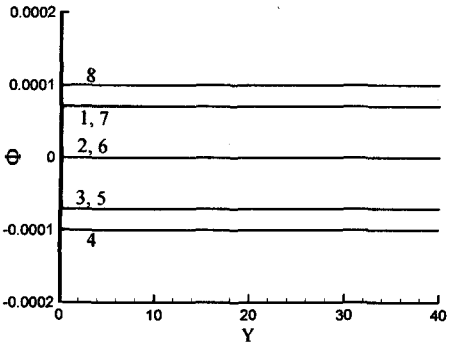

(f)

Fig. 2 Numerical results of the development of (a) c^+ in the inner layer, (b) Φ in the inner layer, (c) c^+ in the middle layer, (d) Φ in the middle layer, (e) c^+ in the outer layer, and (f) Φ in the outer layer at the parameter set $\gamma = 1000$, $A'_\infty = 0.0001$ and simple initial conditions, (44). The number in each line indicates the time instant within one period, e.g. "1" stands for $t = T_p/8$, and "2" for $t = 2T_p/8$, ...etc. Dashed lines in (a) and (c) denote the analytical solutions.

values; $\gamma = 1000$, $A_\infty' = 0.0001$ where A_∞' is the amplitude of the externally applied potential gradient; $\Phi_\infty = A_\infty' \cos t$. We can see that in the inner layer, i.e. within $Y \le 0.12$ approximately as shown in Fig. 2(a) and (b), all the three variables c^+, c^- and Φ show asymptotic approach toward finite values at the region far from this layer (i.e. for the region $Y >> 0.12$ approximately); the development of c^- is the same as c^+ except that there is 180-degree phase difference between them. Each variable's development in time in this layer can be understood from Fig. 3(a); we can see that they develop in time at the same period as the forcing one. But the concentrations develop in highly non-harmonic fashion as can be more clearly seen from